Leukocyte Rolling on P-Selectin: A Three-Dimensional Numerical Study of the Effect of Cytoplasmic Viscosity

Damir B. Khismatullin[†] and George A. Truskey[‡]

[†]Department of Biomedical Engineering, Tulane University, New Orleans, Louisiana; and [‡]Department of Biomedical Engineering, Duke University, Durham, North Carolina

Supporting Material

METHODS

Model development

The viscoelasticity of the nucleus (core) and the cytoplasm (shell) (cf. Fig. 1 *A*) is each described by the Giesekus constitutive relation:

$$\begin{aligned} &\mathbf{\Pi} = -p\mathbf{I} + 2\mu^{(s)}\mathbf{S} + \mathbf{T}, \quad \mathbf{S} = \frac{1}{2}(\nabla\mathbf{v} + \nabla\mathbf{v}^*), \\ &\lambda_1\left[\frac{\partial\mathbf{T}}{\partial t} + (\mathbf{v}\cdot\nabla)\mathbf{T} - (\nabla\mathbf{v})\mathbf{T} - \mathbf{T}(\nabla\mathbf{v})^* + \kappa\mathbf{T}^2\right] + \mathbf{T} = 2\mu^{(p)}\mathbf{S}. \end{aligned} \tag{S1}$$

Here $\mathbf{D}$ is the total stress tensor, $\mathbf{T}$ the extra stress tensor that represents the cytoskeleton contribution to the shear stress, $\mathbf{v} = (v_x, v_y, v_z)$ the velocity vector, $\mathbf{S}$ the rate-of-strain tensor, p thermodynamic pressure, $\mu^{(s)}$ the solvent (cytosol) viscosity, $\mu^{(p)}$ the polymer (cytoskeleton) viscosity, λ_1 the relaxation time, and κ the Giesekus nonlinear parameter, which is greater than zero for shear thinning fluids. Superscript star denotes the transpose operation. Equation (1) combines several important features of previous rheological models of leukocytes (1-5). In the simulation, the polymer viscosity of the nucleus $\mu_n^{(p)}$ is higher than the polymer viscosity of the cytoplasm $\mu_{cp}^{(p)}$. The solvent viscosities of the nucleus and cytoplasm are equal to the extracellular fluid viscosity: $\mu_{cp}^{(s)} = \mu_n^{(s)} = \mu_{ext}$. The cytoplasmic and nuclear viscosities are the sum of the respective polymer and solvent viscosities.

According to Eq. (S1) with $\kappa = 0$, if the shear rate is constant, the apparent viscosity of the leukocyte cytoplasm μ_{cp}^{+} will increase exponentially with time as follows (6):

$$\mu_{cp}^{+} = \left(\mu_{cp}^{(s)} + \mu_{cp}^{(p)}\right)\left[\frac{\mu_{cp}^{(s)}}{\mu_{cp}^{(p)}} + \left(1 - \frac{\mu_{cp}^{(s)}}{\mu_{cp}^{(p)}}\right)\left(1 - e^{-t/\lambda_{1cp}}\right)\right], \tag{S2}$$

i.e., the apparent cytoplasmic viscosity is initially equal to the solvent viscosity $\mu_{cp}^{(s)}$, but it approaches the much higher polymer viscosity $\mu_{cp}^{(p)}$ when time t becomes much larger than the cytoplasmic relaxation time λ_{1c}. Thus, when the cell first contacts the substrate, it experiences large deformation determined by the solvent viscosity, but then its deformation will decrease because of the increase of the apparent viscosity.

In the model, the plasma membrane and the actin cortex form a layer of infinitesimal thickness that possesses cortical tension (7). Cylindrical microvilli are distributed equidistantly over the cell membrane using spherical coordinates centered on the cell (8) and the cubature formulae (9). Cell adhesion molecules that are present on microvilli tips (i.e., PSGL-1) interact with their counterparts (P-selectin) distributed uniformly over the lower surface (substrate) of the rectangular flow channel if the separation distance between a microvillus tip and the substrate is less than or equal to the total length of interacting

molecules $l_r + l_l$ (Fig. 1 *A*). Receptor-ligand bonds respond elastically to external forces, thus generating a pulling force (bond force) on microvilli and the cell body. The flow channel is characterized by length *L*, width *W*, and height *H* (Fig. 1 *B*). The pressure drop ΔP between the inlet and outlet of the channel leads to fully established flow of a Newtonian fluid (saline, growth medium, blood plasma, etc.) that exerts the hydrodynamic force on the leukocyte (Fig. 1 *C*). The motion and deformation of the leukocyte are the result of the balance between the hydrodynamic force, the bond force, the inertial force, and the net external force including gravity.

The following modifications have been made to this solver:

- During initialization, the cubature formulae (9) are used to distribute ligand molecules equidistantly on the hemispherical tip of each microvillus. The global coordinates of these molecules are determined from their local position on the microvillus tip (which we assume does not change with time), the location of the microvillus tip, and the microvillus orientation. Receptor molecules are distributed with known density n_r on the substrate.

- Receptor-ligand interaction is modeled by probabilistic single bond kinetics. In our implementation, if a pair of unbound receptor and ligand molecules is separated by a distance below critical, they form a "soft" bond. A "soft" bond does not exert any force on the cell, but it transforms to a "hard" bond when the probability for bond association P_A exceeds a random value $P_A^{(rand)}$ between 0 and 1. When extended, a "hard" bond generates the pulling force on the microvillus tip. The probability for bond dissociation P_D is calculated and compared with another random value $P_D^{(rand)}$ for both "soft" and "hard" bonds. The bond dissociation occur if $P_D > P_D^{(rand)}$. Note that it is unnecessary to calculate P_A for "hard" bonds. In most runs, we updated the values of $P_A^{(rand)}$ and $P_D^{(rand)}$ every time step for each receptor-ligand pair using the pseudorandom number generator built in Fortran. However, since using random numbers makes the code validation more difficult, both $P_A^{(rand)}$ and $P_D^{(rand)}$ were fixed at 0.5 in the time step refinement study discussed below. With the unstressed values k_{f0} and k_{r0} of the forward and reverse reaction rate coefficients given, the probabilities for bond association and dissociation are found from the following formulae:

$$P_A = 1 - \exp(-k_f n_r \tau), \quad P_D = 1 - \exp(-k_r \tau), \tag{S3}$$

$$k_f = k_{f0} \exp\left(-\frac{\kappa_{ts}(l - l_{b0})^2}{2k_B T} \right), \quad k_r = k_{r0} \exp\left(\frac{(\kappa_b - \kappa_{ts})(l - l_{b0})^2}{2k_B T} \right). \tag{S4}$$

This is similar to what was used in previous computational works (8,10). It should be noted, however, that τ in Eqs. (S3) is not the time step but the time since the formation of a "soft" or "hard" bond. Equations (S3) are the result of the direct integration of Eqs. (A1) and (A2) in Hammer & Apte (8). Also, using the fixed time step in these formulae would lead to the constant value of the dissociation probability for unstressed bonds (i.e., when the off-rate is constant). This makes bond dynamics time step-dependent, with the formation of extremely long-lived bonds at a sufficiently small time step. Receptor-ligand bonds have a finite lifetime independent of whether they are stressed or not. This indicates that the bond dissociation

probability should increase with time. Equations (S4) represent the spring-peeling model for receptor-ligand interaction first proposed by Dembo et al. (11). In our algorithm, these equations are applied only to extended bonds, i.e., when the bond length l exceeds the unstressed bond length l_{b0}. Otherwise, $k_f = k_{f0}$ and $k_r = k_{r0}$. Here, κ_b and κ_{ts} are the bond spring constant and the transition state bond spring constant, respectively; k_B = 1.38×10^{-23} J/K the Boltzmann constant; and T temperature in Kelvin. If $\kappa_{ts} = 0$, the Dembo model is analogous to the Bell model (12):

$$k_f = k_{f0}, \quad k_r = k_{r0} \exp\left(\frac{r_a F_b}{N_b k_B T} \right), \tag{S5}$$

where r_a is the empirical parameter called reactive compliance or potential length (it is typically several angstroms), N_b the total number of bonds on the cell, and F_b the magnitude of the total bond force.

- Microvilli are modeled as massless rods. They do not contribute to the velocity field in the lubrication zone between the cell surface and the substrate. However, receptor-ligand binding at their tips generates the pulling force on the cell. The same approach was used in other numerical algorithms of cell rolling, e.g.., Adhesive Dynamics (8) and a fluid capsule model (10). We do not consider microvilli bending. When they are confined, they can pivot around their base provided their length is equal to the unstressed value. This approach was first used by Pospieszalska and Ley (13).

We take into account the viscoelastic deformation of microvilli and the viscous extension of membrane tethers from these projections when the magnitude of the bond force per microvillus $F_b^{(mv)}$ becomes greater than the threshold value F_0 (14). A microvillus and its receptor-ligand bonds form a spring in series. The length l_s and orientation $\mathbf{n}_s$ of a microvillus-bond spring are determined every time step from the microvillus coordinates on the cell body and the average of its "hard" bonds coordinates on the substrate. By subtracting the instantaneous length l_{mv} of a microvillus, determined at the previous time step, from the microvillus-bond spring length, we find the coordinates $(x_{tip}, y_{tip}, z_{tip})$ of the microvillus tip and the instantaneous lengths l_{bi} of all bonds on this microvillus. The bond force per microvillus $\mathbf{F}_b^{(mv)}$ is the sum of Hookean forces:

$$\mathbf{F}_b^{(mv)} = -\sum_i \gamma \kappa_b (l_{bi} - l_{b0}) \mathbf{n}_{bi} \tag{S6}$$

where $\mathbf{n}_{bi}$ is the unit vector showing ith bond orientation and $\gamma > 1$ is the force amplification factor that accounts for entropic elasticity of cell adhesion molecules (15) and the fact that P-selectin/PSGL-1 bonds are dimeric (16). The evidence that the spring constant for bond kinetics κ_b is less than the spring constant for bond force $\gamma\kappa_b$ comes from matching the Dembo and Bell models and taking into account that the reactive compliance r_a is less than the bond extension $l - l_{b0}$. Also, if $\gamma = 1$ and $\kappa_{ts} = 0$, Eqs. (S3) and (S4) predict that the P-selectin/PSGL-1 rupture force at the experimental time scale of 40 ms (15) and the unstressed

off-rate $k_{r0} = 1$ s^{-1} (17) is 27.3 pN, while the experimental data indicate that this force is 165 pN and higher (15,18).

We use the Kelvin-Voigt (viscoelastic solid) model for microvillus extension (13). According to this model, the instantaneous length of a microvillus is calculated as

$$l_{mv} = l_{mv0} + \frac{F_b^{(mv)}}{\kappa_{mv}} - \left(\frac{F_b^{(mv)}}{\kappa_{mv}} - l_{mv}^{(ve)} + l_{mv0} \right) \exp\left(-\Delta t / \lambda_{mv}\right) + l_{tether}. \qquad \text{(S7)}$$

Here l_{mv0} is the unstressed length of a microvillus, $l_{mv}^{(ve)}$ the microvillus length at the previous time step minus the tether length l_{tether}, κ_{mv} the microvillus spring constant, $\lambda_{mv} = \mu_{mv} / \kappa_{mv}$ the microvillus relaxation time, μ_{mv} the microvillus viscosity, and Δt is the time step. Assuming that the tether behaves as a Newtonian fluid with viscosity μ_{tether}, its length is determined from the following equation (13,14):

$$\mu_{tether}(dl_{tether} / dt) = F_b^{(mv)} - F_0. \qquad \text{(S8)}$$

- To simulate deformable cell rolling in shear flow, we solved the full form of the Navier-Stokes equations (i.e., including both viscoelastic and inertial terms) by using the predictor-corrector approach for improved numerical accuracy:

$$\rho\left(\frac{\partial \mathbf{v}}{\partial t} + \mathbf{v} \cdot \nabla \mathbf{v}\right) = -\nabla p + \nabla \cdot (\mu^{(s)}(\nabla \mathbf{v} + (\nabla \mathbf{v})^T)) + \nabla \cdot \mathbf{T} + \mathbf{f}_b + \mathbf{f}_{ct} + \rho \mathbf{g} \qquad \text{(S9)}$$

($\mathbf{f}_b$ is the total microvillus-bond force per unit volume of the cell, $\mathbf{f}_{ct}$ the force due to cortical tension per unit volume of the cell, $\mathbf{g}$ the acceleration due to gravity, and ρ the cell or fluid density). Specifically, we first use the explicit scheme for the intermediate velocity in Chorin's projection method (19) and, based on this velocity; we find the pressure field by the multigrid solver. Then, we recalculate the intermediate velocity field via a semi-implicit scheme using this intermediate pressure field. The final correction to the pressure is found by the multigrid solver. The resulting velocity field at the given time step is determined by adding the gradient of the total pressure to the intermediate velocity.

Although we do not expect that fluid inertia contributes substantially to the rolling process at low shear stresses considered in this study, its role could be important at high shear stresses existing, e.g., in the problem of monocyte adhesion to arterial endothelium at atherosclerosis-prone sites.

- In the new algorithm, inflow/outflow boundary conditions are applied to the velocity field. In particular, the velocity field at the inlet and outlet and the initial velocity field are calculated from the series solution for fully developed flow in a rectangular duct (20):

$$U_x = \frac{4k^2}{\pi^3} \frac{H^2 \Delta P}{\mu_f L} \sum_{n=0}^{N} \frac{(-1)^n}{(2n+1)^3} \left[1 - \frac{\cosh\left(\frac{2n+1}{k} \cdot \pi z_1 \right)}{\cosh\left(\frac{2n+1}{2k} \cdot \pi \right)} \right] \cos\left((2n+1)\pi y_1\right), \qquad \text{(S10)}$$

$$U_y = U_z = 0, \tag{S11}$$

where L, W, H are the length, width, and height of the channel (cf. Fig. 1 *B*); $z_1 = (z - H/2)/H$, $y_1 = (y - W/2)/W$, $k = W/H$; μ_f is the viscosity of bulk (extracellular) fluid; and ΔP the pressure drop between the inlet and the outlet. In all runs, $N = 100$. Equation (S10) leads to the following formula for the perimeter-average wall shear stress (WSS):

$$\tau_w = \frac{\Delta P}{2L}\left(\frac{WH}{W+H}\right). \tag{S12}$$

The leukocyte is initially positioned >2.5 diameters away from the inlet and the numerical simulation stops or the computational domain moves forward before the leading edge of the cell is two cell diameters away from the outlet. This ensures that the flow disturbances produced by the cell do not reach both the inlet and the outlet (21). The initial *z*-coordinate of the cell centroid z_c was selected below the threshold value $R + l_{mv0} + l_r + l_l$ at which the separation distance between the cell surface and the substrate is equal to the unstressed microvillus length + the total length of receptor and ligand molecules. If z_c were larger than this threshold value, the cell would never attach to the substrate and thus would freely move in the channel. In the tethering stage, when the contact area increases, the separation distance decreases with time until the minimum separation distance greater than zero is reached. Please note that we did not observe any substantial changes in the mean rolling velocity or cell-substrate contact area with z_c below the threshold.

Input and output of the model

Most of the input parameters are in the range of experimental measurements for human monocytes and neutrophils (Table 1). These include the radius and nuclear volume fraction (1), density (22), number and length of microvilli (23,24), microvillus tip radius (12), and mechanical properties of microvilli and their tethers (14). The total number of PSGL-1 molecules per cell was 17×729=12,393. Human neutrophils express between 10,000 and 30,000 PSGL-1 molecules per cell (25,26), with 80% of molecules located on microvilli tips (27). The P-selectin density had the same value (145 molecules μm^{-2}) as in parallel-plate flow experiments by Yago et al. (28), which were used to test the numerical data. The contour lengths of the extracellular parts of P-selectin and PSGL-1 molecules were respectively 40 nm and 45 nm (29,30), but we assumed that this pair of molecules was not in the fully extended configuration when their bonded state reached equilibrium, i.e., the unstressed (equilibrium) bond length $l_{b0} = 70$ nm (13) was less than the total contour length $l_r + l_l = 85$ nm. P-selectin/PSGL-1 bonds were characterized by the spring constant $\kappa_b = 5.3$ pN nm^{-1}, according to Fritz et al. (15), and we also considered a small transition state spring constant $\kappa_{ts} = 0.1$ pN nm^{-1} (11). Thus, we have the case of slip bonds far from ideal bonds ($\kappa_b >> \kappa_{ts}$) when the Dembo model approaches the experimentally-tested Bell model [cf. Eqs. (S4) and (S5)].

The cytoplasmic viscosity μ_{cp} of the leukocyte varied in the simulation from 5 to 100 Pa s (50 to 1000 poise), based on micropipette aspiration data (1-3,7,31-33). The solvent

viscosity of the cytoplasm (i.e., the cytosol viscosity) and the solvent viscosity of the nucleus were equal to the extracellular fluid viscosity. Since no measurement exists for the nuclear viscosity, we used numbers determined for other cell types. Particularly, the nuclear viscosity of a Swiss 3T3 fibroblast is more than twice the cytoplasmic viscosity, according to multiple-particle nanotracking studies (34). In most runs, the nucleus-to-cytoplasm viscosity ratio $\mu_n / \mu_{cp} = 2.5$, but we also consider the cases of $\mu_n / \mu_{cp} =$ 1 and 10. The base value of cortical tension T_c is 30 μN m^{-1}, according to micropipette aspiration data (3,35). In the analysis of the cortical tension effect, we also consider T_c = 0, 100, and 300 μN m^{-1}.

The output of the computational model includes 1) the shape of the cell body and nucleus; 2) microvilli bases coordinates and microvilli lengths; 3) the number of "soft" and "hard" bonds, bond lengths, and tether length for each attached microvillus; 4) the hydrodynamic force $\mathbf{F}_h(t)$, the total bond force $\mathbf{F}_b(t)$, and the force due to cortical tension $\mathbf{F}_{ct}(t)$ experienced by the cell; and 5) the velocity, pressure, and stress fields in the whole computational domain. Microvilli data were further analyzed by a custom post-processing code (cf. below) to determine the deformation index and velocity of the cell at different time instants. Regression and statistical analysis of the numerical data and data plotting were performed with GraphPad Prism ver. 5.0 (GraphPad Software, San Diego, CA). The numerical code was run four to six times for each viscosity case, i.e., we simulated four to six cells for each value of the cytoplasmic viscosity.

Time step refinement

In all runs, the width and height of the computational domain were 15 μm each, less than the channel width and height (2.5 cm and 500 μm). The computational domain was positioned such that its lower surface and its mid-plane in the *y*-direction coincided with those of the channel. The number of grid cells for the (60 μm, 15 μm, 15 um) domain were 128×32×32.

To determine the step that is small enough to accurately model cell rolling, we ran our algorithm with $P_A^{(rand)} = P_D^{(rand)} = 0.5$ and time steps ranging from 0.1 to 1.0 μs. In this deterministic simulation, we considered two values of the cytoplasmic viscosity: 50 and 300 P. Since we were unable to observe cell capture and rolling directly from the flow when $P_A^{(rand)}$ was fixed at 0.5, we were first exposed the cells to no flow conditions for 0.5 s and then continued the simulation for next 1.25 s with the WSS of 0.5 dyn/cm^2. Table S1 shows the results of the time step refinement study. An increase in the time step leads to an increase in the time variability of the cell rolling velocity (measured by the standard deviation (SD) of the velocity data). The mean rolling velocity changes insignificantly for all cells when Δt increases from 0.1 to 0.5 μs. An increase in the time step to 1.0 μs has an insignificant effect on rolling of a 50 P-viscosity cell, but a more viscous (300 P) cell detaches. Based on this result, we ran our stochastic simulations with the time step equal or less than 0.5 μs. Specifically, we used Δt = 0.5 μs for the cytoplasmic viscosity of 50 to 300 P, 0.25 μs for 500 P, and 0.1 μs for 1000 P. We should also mention that the viscoelastic part of our algorithm was already validated against the experimental data on drop breakup (36).

Post-processing

The deformation index $D_{cell}(t)$ of the leukocyte was calculated from the following formula:

$$D_{cell}(t) = \frac{1}{N_{cell}} \sum_{i=1}^{N_{cell}} l_{\max}^{(i)}(t) / l_{\min}^{(i)}(t), \tag{S13}$$

where N_{cell} is the number of independent runs; $l_{\max}^{(i)}(t)$ and $l_{\min}^{(i)}(t)$ are the maximum and minimum lengths of the cell in run i estimated from the coordinates of microvilli bases $(x_{mv}^{(j)}(t), y_{mv}^{(j)}(t), z_{mv}^{(j)}(t))$, $j = 1, 2, \ldots, N_{mv}$; and N_{mv} is the number of microvilli per cell. Equation (1) is closely related to the deformation index used in work by Damiano et al. (37) to analyze the deformation of rolling leukocytes in vivo.

The instantaneous velocity $U_{cell}(t)$ of the cell was determined by the following expression:

$$U_{cell}(t) = \frac{x_c(t) - x_c(t - \Delta t)}{\Delta t}, \quad x_c(t) = \frac{1}{N_{mv}} \sum_{j=1}^{N_{mv}} x_{mv}^{(j)}(t), \tag{S14}$$

where $x_c(t)$ and $x_c(t - \Delta t)$ are the x-coordinate of the cell centroid at the current and previous time steps. The rolling velocity $U_{roll}(t)$ is the average instantaneous velocity 1) over the time period T = 0.5 s and 2) over all independent runs, i.e.,

$$U_{roll}(t) = \frac{1}{N_{cell} T} \sum_{i=1}^{N_{cell}} \sum_{k=1}^{N_T} U_{cell}^{(i)}(t - (N_T - k)\Delta t), \quad N_T = \text{trunc}(T / \Delta t). \tag{S15}$$

The mean rolling velocity $< U_{roll}(t) >$ and the mean deformation index $< D_{cell}(t) >$ were calculated by averaging the rolling velocity and deformation index data from the time t_{qss} when a quasi steady state for cell rolling is reached to the time t_{final} when the simulation ends or the cell detaches.

The boundary curve for the cell-substrate contact region was approximated as an ellipse with the major diameter $2a = x_{mv}^{(\max)}(t) - x_{mv}^{(\min)}(t)$ and the minor diameter $2b = y_{mv}^{(\max)}(t) - y_{mv}^{(\min)}(t)$, where superscripts "max" and "min" indicate the coordinates of the attached microvilli located farthest from the cell centroid in respectively the positive and negative directions along x- or y-axes. Then, the contact area $A_{cell}(t)$ is equal to

$$A_{cell}(t) = \frac{\pi}{4N_{cell}} \sum_{i=1}^{N_{cell}} [x_{mv}^{(\max)}(t) - x_{mv}^{(\min)}(t)]^{(i)} [y_{mv}^{(\max)}(t) - y_{mv}^{(\min)}(t)]^{(i)}. \tag{S16}$$

where superscript "(i)" indicates run i. The hydrodynamic force and the forces exerted on the cell body by receptor-ligand binding and cortical tension were found by integrating $\nabla \cdot \mathbf{\Pi}$, $\mathbf{f}_b$, and $\mathbf{f}_c$, respectively [cf. Eqs. (1) and (7)], over the volume of the cell, i.e.,

$$\mathbf{F}_h(t) = \int_V (\nabla \cdot \mathbf{\Pi}) C dV, \quad \mathbf{F}_b(t) = \int_V \mathbf{f}_b C dV, \quad \mathbf{F}_{ct}(t) = \int_V \mathbf{f}_{ct} C dV. \tag{S17}$$

Here $C = C(t, x, y, z)$ is the concentration (volume fraction) function that takes the value of 1 inside the cell and 0 outside the cell, V the volume of the computational domain. The *x*- and *z*-components of the hydrodynamic force $\mathbf{F}_h(t)$ represent the drag and lift forces, respectively. Note that our formulation of these forces includes the contribution of intracellular viscoelastic stresses.

RESULTS (not included in the main manuscript)

Cell shape

When a free-flowing, deformable cell that behaves as a viscoelastic material initially contacts an adhesive substrate, the bond force balances the hydrodynamic and cortical tension forces leading to elongation of the cell body in the flow direction, enlargement of the cell-substrate contact area due to flattening of the cell bottom, and deceleration of the cell (Fig. S1 *A*). This "tethering" stage continues until cell rolling reaches a quasi steady state, characterized by shape and velocity fluctuations around corresponding equilibrium values. Elongation and flattening of the cell eventually change its initially spherical shape to a tear-drop shape, which is a feature of rolling leukocytes in vivo (cf. Fig. S1 *B* and animations of numerically simulated rolling of the cell).

Cellular deformation reaches a quasi steady state when the cell viscosity is 300 P or less (Fig. S2 *A*). The mean deformation index of the leukocyte decreases from 1.14 to 1.00 (no deformation) when the cytoplasmic viscosity increases from 50 P to 1000 P (Fig. S2 *B*). The time to reach the quasi steady state t_{qss} decreases with an increase in the viscosity, and is approximately equal to 2.0 s for 50 P and 100 P, 1.5 s for 200 P, and 1.0 s for 300 P. Establishment of cell rolling is limited by cellular deformation because it takes less time to reach the time-averaged mean rolling velocity than to reach the equilibrium value for the deformation index (cf. top plot in Fig. S2 *A* and Fig. 5 *D*). A decrease in the deformation index for the 500 P-viscosity cell after t = 1.5 s is an indication that this cell will detach from the substrate. Thus, for a given fluid shear stress (0.5 dyn cm^{-2}) and receptor density (145 sites μm^{-2}), there exists a critical cytoplasmic viscosity (> 300 P) for leukocyte rolling.

Hydrodynamic and bond forces

The mean drag and lift forces on the cell were determined by averaging the force data from the time to reach the quasi steady state t_{qss} to the final time of simulation for multiple runs of the algorithm. An increase in the cytoplasmic viscosity from 50 P to 1000 P increases the mean drag force from 4 pN to 66 pN (Fig. S3 *A*). The mean lift force on low-viscosity cells that roll stably is almost twice less than the corresponding force on high-viscosity cells that eventually detach from the substrate: 101 pN at 200 P and 189 pN at 1000 P (Fig. S3 *B*). When load-bearing bonds on a high-viscosity cell or a rigid bead rupture but there is an insufficient amount of unstressed bonds to quickly replenish it, the lubrication pressure causes an increase in the *z*-component of the cell velocity. With these changes, the probability for cell detachment increases.

Comparison with experiment

The geometry and parameter values of the model considered in our work corresponds to the conditions of in vitro experiments of Yago et al. (28). According to that study, human neutrophils roll on a P-selectin-coated substrate in a parallel-plate flow chamber with the mean velocity of 4 μm s^{-1} at the P-selectin density of 145 sites μm^{-2} and the WSS of 0.5 dyn cm^{-2}. Our model predicts similar values of the mean rolling velocity under these conditions: 2.5 to 5.1 μm s^{-1} when the leukocyte cytoplasmic viscosity is within the range of 50 to 300 P (Fig. 3).

A side-view flow channel is the only *in vitro* technique that permits quantification of rolling cell deformation for rectangular flow geometry (38), but it was never applied to human peripheral leukocytes. In the case of cylindrical flow geometry, Porter and Damiano (unpublished) imaged rolling neutrophils during the perfusion of whole blood in endothelium-lined collagen microvascular tubes (39). Their images give the deformation index of 1.9 for neutrophils at the WSS of 6.2 dyn cm^{-2} (Fig. S4). Since the deformation index of rolling leukocytes in vivo increases approximately linearly with the WSR between 200 and 1500 s^{-1}, according to Fig. 2 in (37), we can estimate the neutrophil deformation index at other values of the WSS using a simple linear expression: $D_{cell} = 1 + k\tau_{w0}$, where τ_{w0} is the WSS and $k = (1.9-1)/6.2 \approx 0.145$ cm^2 dyn^{-1}. This gives $D_{cell} \approx 1.073$ at the WSS of 0.5 dyn cm^{-2}, which is in the range of values predicted by the computational model for the cells with viscosity of 50 to 300 P (cf. Fig. S2).

Table S1. Sensitivity of the computed time-averaged rolling velocity (mean ± SD) to the time step Δt. In this simulation, all Monte Carlo thresholds are fixed at 0.5 and the flow starts at *t* = 0.5 s (detachment assay).

Viscosity (Pa)	$\Delta t = 0.10\ \mu s$	$\Delta t = 0.25\ \mu s$	$\Delta t = 0.50\ \mu s$	$\Delta t = 1.0\ \mu s$
50	3.412 ± 2.288 *μ*m/s	3.317 ± 1.843 *μ*m/s	3.341 ± 3.816 *μ*m/s	3.592 ± 5.472 *μ*m/s
300	3.535 ± 3.644 *μ*m/s	3.687 ± 5.004 *μ*m/s	4.066 ± 7.102 *μ*m/s	detachment

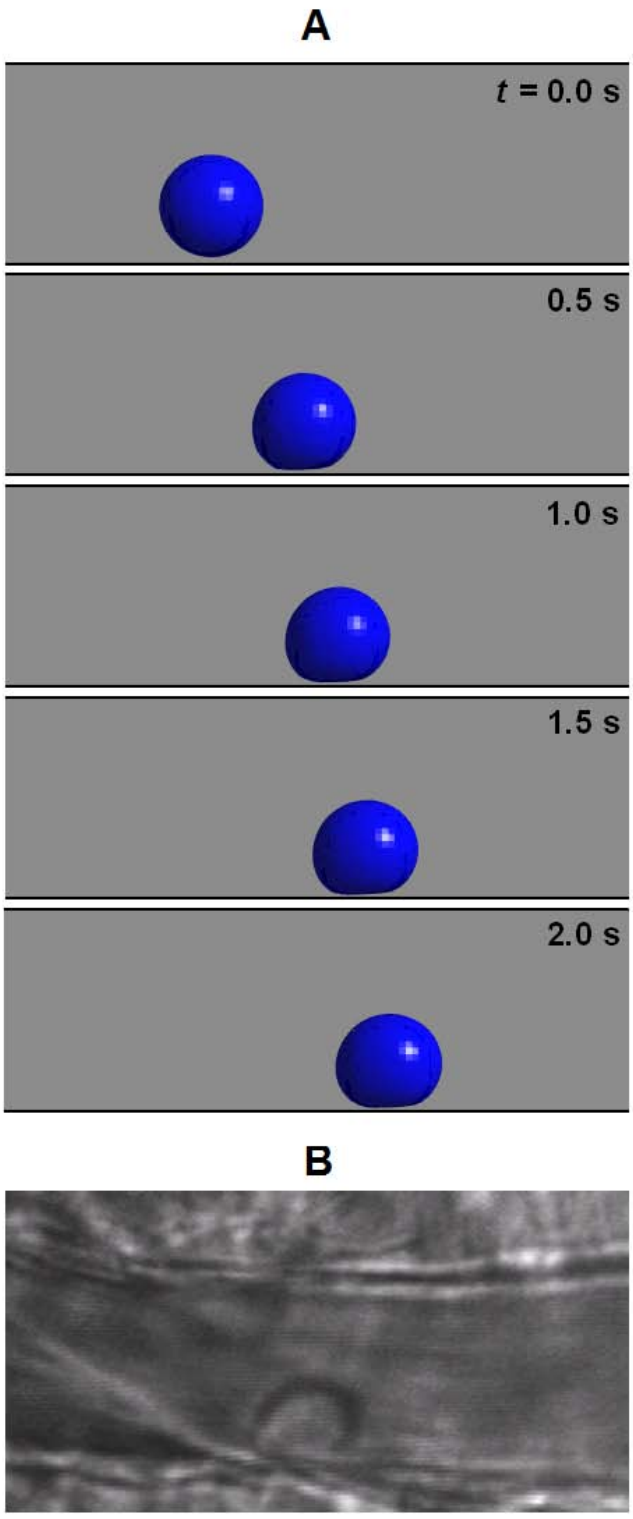

Fig. S1. (A) Snapshots showing shape changes of a leukocyte (side view) in the tethering stage, according to numerical simulations. The viscosity of leukocyte cytoplasm is 100 P. Other parameters are listed in Table 1. (B) A videomicrograph frame showing leukocyte rolling along a postcapillary venule in the mouse cremaster muscle. The flow is from left to right. From (31), with permission.

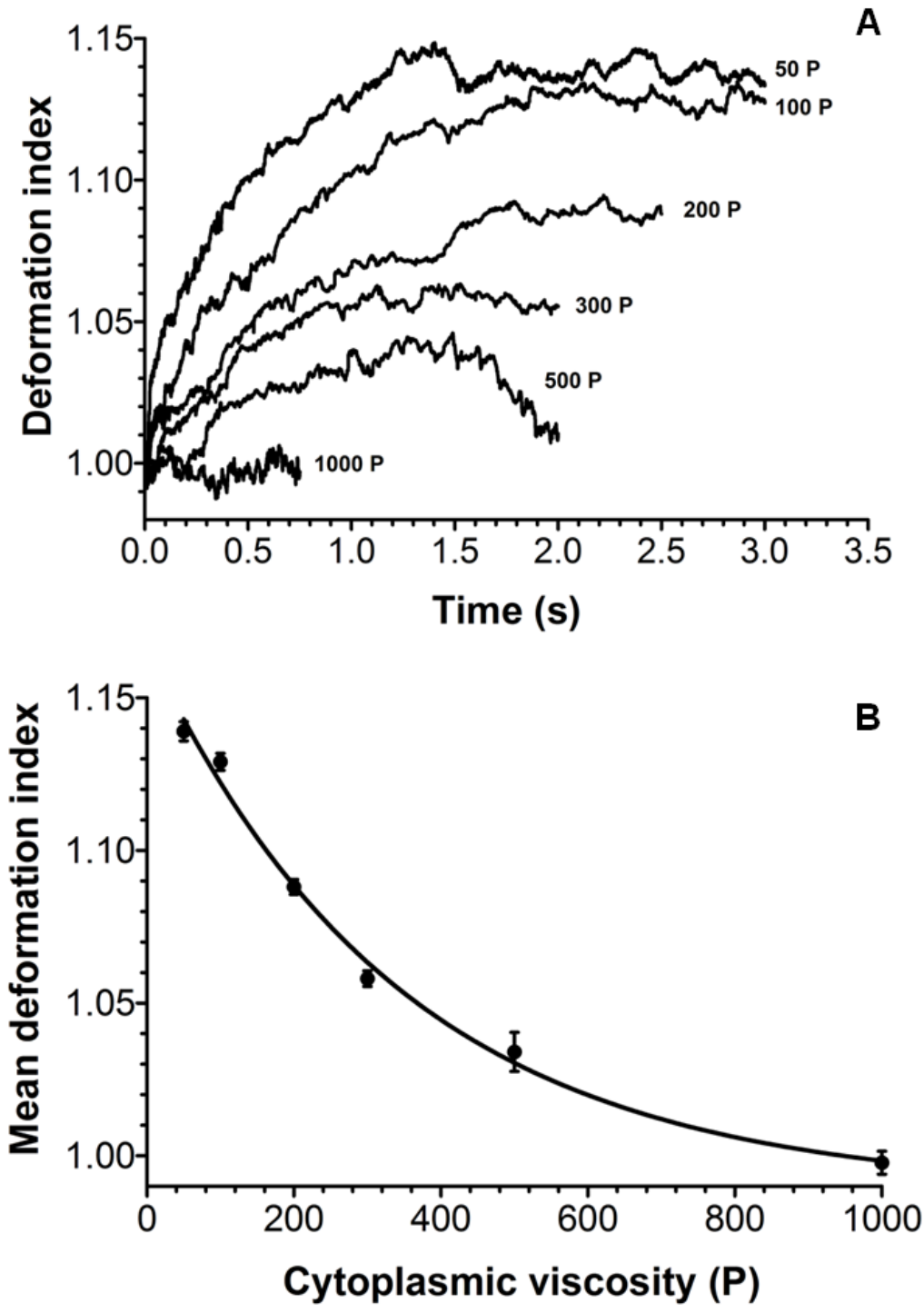

Fig. S2. (A) Deformation index of a rolling leukocyte as a function of time for different values of the cytoplasmic viscosity and a wall shear stress of 0.5 dyn cm^{-2}, according to numerical simulations. (B) The mean deformation index vs. cytoplasmic viscosity curve indicates that higher-viscosity cells are less deformable.

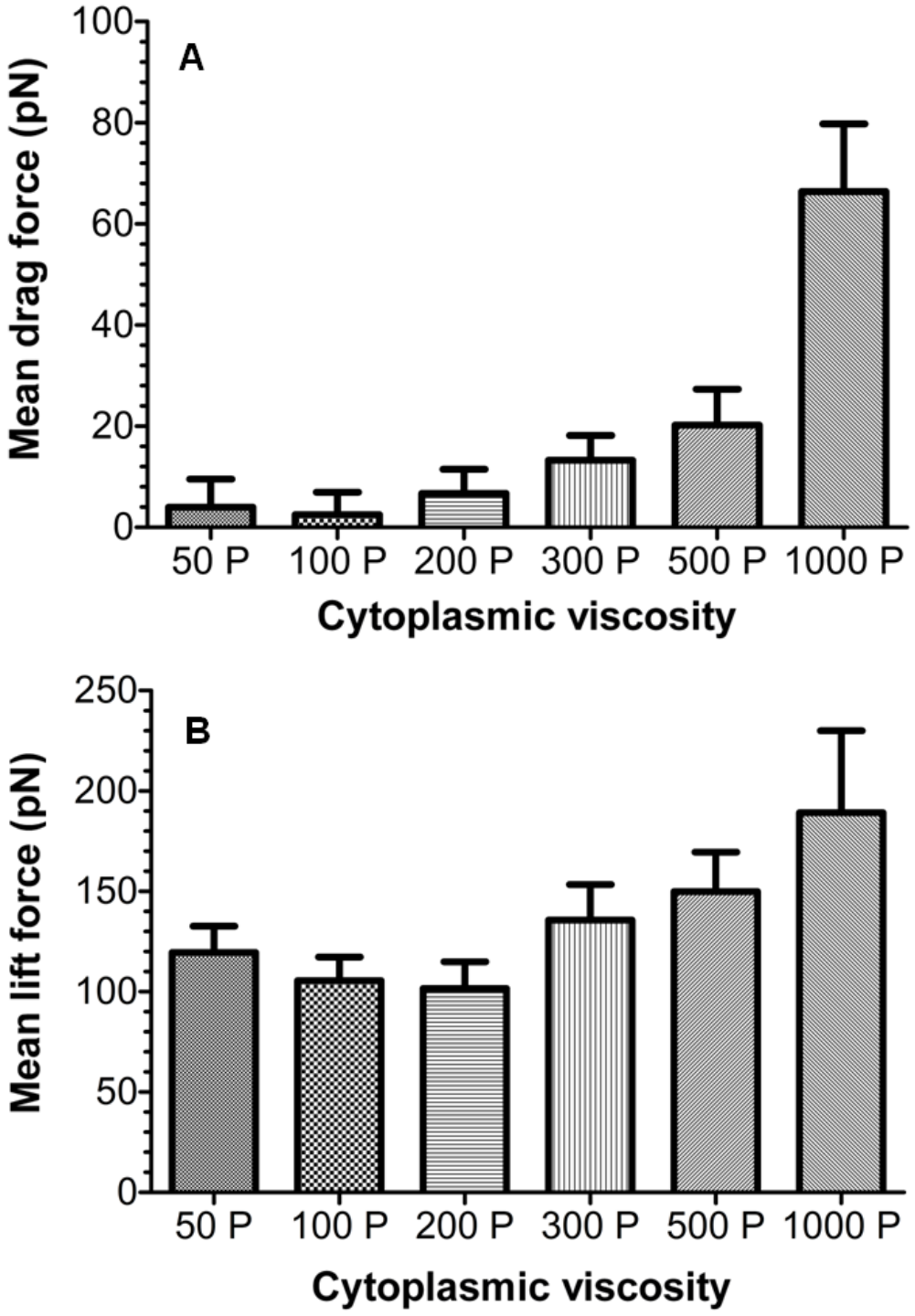

Fig. S3. (A) Mean drag force and (B) mean lift force on a rolling cell as a function of the cytoplasmic viscosity. An increase in the cell viscosity leads to an increase in the hydrodynamic force due to a higher bond force experienced by the cell and lesser deformability of the cell.

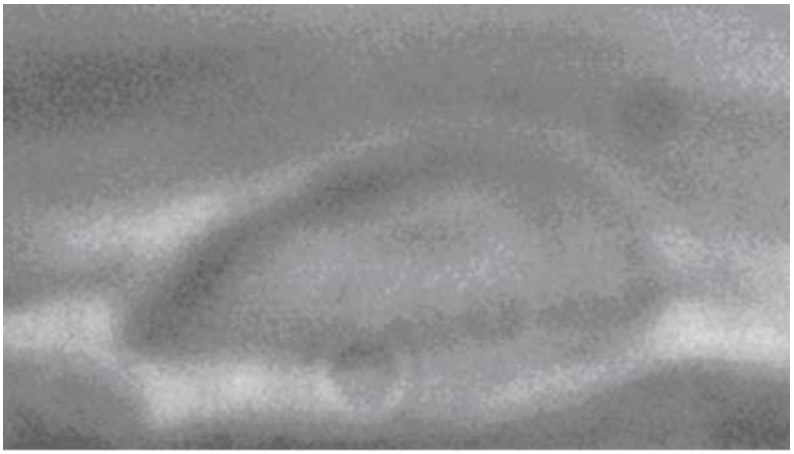

Fig. S4. Image of human neutrophil rolling along TNF-α-activated HUVEC during the whole blood perfusion. In vitro collagen tube assay. The wall shear stress is about 6.20 dyn/cm^2. Provided by D. Potter and E. Damiano (Boston University).

SUPPORTING REFERENCES

1. Schmid-Schonbein, G. W., K. L. Sung, H. Tozeren, R. Skalak, and S. Chien. 1981. Passive mechanical properties of human leukocytes. Biophys J 36:243-256.

2. Dong, C., R. Skalak, K. L. Sung, G. W. Schmid-Schonbein, and S. Chien. 1988. Passive deformation analysis of human leukocytes. J Biomech Eng 110:27-36.

3. Tsai, M. A., R. S. Frank, and R. E. Waugh. 1993. Passive mechanical behavior of human neutrophils: power-law fluid. Biophys J 65:2078-2088.

4. Drury, J. L. and M. Dembo. 2001. Aspiration of human neutrophils: effects of shear thinning and cortical dissipation. Biophys J 81:3166-3177.

5. Zhou, C., P. Yue, and J. J. Feng. 2007. Simulation of neutrophil deformation and transport in capillaries using newtonian and viscoelastic drop models. Ann Biomed Eng 35:766-780.

6. Bird, R. B., R. C. Armstrong, and O. Hassager. 1987. Dynamics of Polymeric Liquids. Vol. 1: Fluid Mechanics. New York: Wiley.

7. Evans, E. and A. Yeung. 1989. Apparent viscosity and cortical tension of blood granulocytes determined by micropipet aspiration. Biophys J 56:151-160.

8. Hammer, D. A. and S. M. Apte. 1992. Simulation of cell rolling and adhesion on surfaces in shear flow: general results and analysis of selectin-mediated neutrophil adhesion. Biophys J 63:35-57.

9. Fliege, J. and U. Maier. 1999. The distribution of points on the sphere and corresponding cubature formulae. IMA Journal of Numerical Analysis 19:317-334.

10. Jadhav, S., C. D. Eggleton, and K. Konstantopoulos. 2005. A 3-D computational model predicts that cell deformation affects selectin-mediated leukocyte rolling. Biophys J 88:96-104.

11. Dembo, M., D. C. Torney, K. Saxman, and D. Hammer. 1988. The reaction-limited kinetics of membrane-to-surface adhesion and detachment. Proc R Soc Lond B Biol Sci 234:55-83.

12. Bell, G. I. 1978. Models for the specific adhesion of cells to cells. Science 200:618-627.

13. Pospieszalska, M. K. and K. Ley. 2009. Dynamics of Microvillus Extension and Tether Formation in Rolling Leukocytes. Cell Mol Bioeng 2:207-217.

14. Shao, J. Y., H. P. Ting-Beall, and R. M. Hochmuth. 1998. Static and dynamic lengths of neutrophil microvilli. Proc Natl Acad Sci U S A 95:6797-6802.

15. Fritz, J., A. G. Katopodis, F. Kolbinger, and D. Anselmetti. 1998. Force-mediated kinetics of single P-selectin/ligand complexes observed by atomic force microscopy. Proc Natl Acad Sci U S A 95:12283-12288.

16. Marshall, B. T., K. K. Sarangapani, J. Lou, R. P. McEver, and C. Zhu. 2005. Force history dependence of receptor-ligand dissociation. Biophys. J. 88:1458-1466.

17. Alon, R., D. A. Hammer, and T. A. Springer. 1995. Lifetime of the P-selectin-carbohydrate bond and its response to tensile force in hydrodynamic flow. Nature 374:539-542.

18. Lawrence, M. B. and T. A. Springer. 1991. Leukocytes roll on a selectin at physiologic flow rates: distinction from and prerequisite for adhesion through integrins. Cell 65:859-873.

19. Chorin, A. J. 1967. A numerical method for solving incompressible viscous flow problems. J. Comp. Phys. 2:12 - 26.

20. Loitsyanskii, L. G. 1966. Mechanics of Liquids and Gases Burlington: Elsevier.

21. Lan, H. and D. B. Khismatullin. 2012. A Numerical Study of the Lateral Migration and Deformation of Drops and Leukocytes in a Rectangular Microchannel. Int. J. Multiphase Flow (submitted).

22. Zipursky, A., E. Bow, R. S. Seshadri, and E. J. Brown. 1976. Leukocyte density and volume in normal subjects and in patients with acute lymphoblastic leukemia. Blood 48:361-371.

23. Bruehl, R. E., T. A. Springer, and D. F. Bainton. 1996. Quantitation of L-selectin distribution on human leukocyte microvilli by immunogold labeling and electron microscopy. J Histochem Cytochem 44:835-844.

24. Majstoravich, S., J. Zhang, S. Nicholson-Dykstra, S. Linder, W. Friedrich, K. A. Siminovitch, and H. N. Higgs. 2004. Lymphocyte microvilli are dynamic, actin-dependent structures that do not require Wiskott-Aldrich syndrome protein (WASp) for their morphology. Blood 104:1396-1403.

25. Moore, K. L., N. L. Stults, S. Diaz, D. F. Smith, R. D. Cummings, A. Varki, and R. P. McEver. 1992. Identification of a specific glycoprotein ligand for P-selectin (CD62) on myeloid cells. J Cell Biol 118:445-456.

26. Norman, K. E., A. G. Katopodis, G. Thoma, F. Kolbinger, A. E. Hicks, M. J. Cotter, A. G. Pockley, and P. G. Hellewell. 2000. P-selectin glycoprotein ligand-1 supports rolling on E- and P-selectin in vivo. Blood 96:3585-3591.

27. Bruehl, R. E., K. L. Moore, D. E. Lorant, N. Borregaard, G. A. Zimmerman, R. P. McEver, and D. F. Bainton. 1997. Leukocyte activation induces surface redistribution of P-selectin glycoprotein ligand-1. J Leukoc Biol 61:489-499.

28. Yago, T., A. Leppanen, H. Qiu, W. D. Marcus, M. U. Nollert, C. Zhu, R. D. Cummings, and R. P. McEver. 2002. Distinct molecular and cellular contributions to stabilizing selectin-mediated rolling under flow. J Cell Biol 158:787-799.

29. Ushiyama, S., T. M. Laue, K. L. Moore, H. P. Erickson, and R. P. McEver. 1993. Structural and functional characterization of monomeric soluble P-selectin and comparison with membrane P-selectin. J Biol Chem 268:15229-15237.

30. Li, F., H. P. Erickson, J. A. James, K. L. Moore, R. D. Cummings, and R. P. McEver. 1996. Visualization of P-selectin glycoprotein ligand-1 as a highly extended molecule and mapping of protein epitopes for monoclonal antibodies. J Biol Chem 271:6342-6348.

31. Khismatullin, D. B. 2009. The Cytoskeleton and Deformability of White Blood Cells. In Leukocyte Rolling and Adhesion: Current Topics in Membranes. Vol. 64. K. Ley, editor. Academic Press. 47-111.

32. Hochmuth, R. M., H. P. Ting-Beall, B. B. Beaty, D. Needham, and R. Tran-Son-Tay. 1993. Viscosity of passive human neutrophils undergoing small deformations. Biophys J 64:1596-1601.

33. Needham, D. and R. M. Hochmuth. 1990. Rapid flow of passive neutrophils into a 4 microns pipet and measurement of cytoplasmic viscosity. J Biomech Eng 112:269-276.

34. Tseng, Y., J. S. Lee, T. P. Kole, I. Jiang, and D. Wirtz. 2004. Micro-organization and visco-elasticity of the interphase nucleus revealed by particle nanotracking. J Cell Sci 117:2159-2167.

35. Zhelev, D. V., D. Needham, and R. M. Hochmuth. 1994. Role of the membrane cortex in neutrophil deformation in small pipets. Biophys J 67:696-705.

36. Khismatullin, D., Y. Renardy, and M. Renardy. 2006. Development and implementation of VOF-PROST for 3D viscoelastic liquid-liquid simulations. Non-Newt Fluid Mech 140:120-131.

37. Damiano, E. R., J. Westheider, A. Tozeren, and K. Ley. 1996. Variation in the velocity, deformation, and adhesion energy density of leukocytes rolling within venules. Circ Res 79:1122-1130.

38. Leyton-Mange, J., S. Yang, M. H. Hoskins, R. F. Kunz, J. D. Zahn, and C. Dong. 2006. Design of a side-view particle imaging velocimetry flow system for cell-substrate adhesion studies. J Biomech Eng 128:271-278.

39. Chrobak, K. M., D. R. Potter, and J. Tien. 2006. Formation of perfused, functional microvascular tubes in vitro. Microvasc Res 71:185-196.